Optics Communications 381 (2016) 10–17

Contents lists available at ScienceDirect

Optics Communications

journal homepage: www.elsevier.com/locate/optcom

Integration of variable-rate OWC with OFDM-PON for hybrid optical access based on adaptive envelope modulation

Chen Chen *, Wen-De Zhong, Dehao Wu

School of Electrical and Electronic Engineering, Nanyang Technological University, 50 Nanyang Avenue, 639798 Singapore

ARTICLE INFO

Article history:
Received 25 April 2016
Received in revised form
17 June 2016
Accepted 22 June 2016
Available online 4 July 2016

Keywords:
Hybrid optical access
Passive optical network
Orthogonal frequency division multiplexing
Optical wireless communication
Adaptive envelope modulation

ABSTRACT

In this paper, we investigate an integrated optical wireless communication (OWC) and orthogonal frequency division multiplexing based passive optical network (OFDM-PON) system for hybrid wired and wireless optical access, based on an adaptive envelope modulation technique. Both the outdoor and indoor wireless communications are considered in the integrated system. The data for wired access is carried by a conventional OFDM signal, while the data for wireless access is carried by an *M*-ary pulse amplitude modulation (*M*-PAM) signal which is modulated onto the envelope of a phase-modulated OFDM signal. By adaptively modulating the wireless *M*-PAM signal onto the envelope of the wired phase-modulated constant envelope OFDM (CE-OFDM) signal, hybrid wired and wireless optical access can be seamlessly integrated and variable-rate optical wireless transmission can also be achieved. Analytical bit-error-rate (BER) expressions are derived for both the CE-OFDM signal with *M*-PAM overlay and the overlaid unipolar *M*-PAM signal, which are verified by Monte Carlo simulations. The BER performances of wired access, indoor OWC wireless access and outdoor OWC wireless access are evaluated. Moreover, variable-rate indoor and outdoor optical wireless access based on the adaptive envelope modulation technique is also discussed.

1. Introduction

Next generation access networks are expected to provide high-speed hybrid wired and wireless services for end users [1,2]. Due to its low cost, high capacity and easy upgradability, passive optical network (PON) has been considered as a promising candidate for high-speed wired access [3–5]. In recent years, orthogonal frequency division multiplexing based PON (OFDM-PON) has attracted tremendous attention, since OFDM has high spectral efficiency, robustness to chromatic dispersion and flexibility of dynamic bandwidth allocation [6–8]. Moreover, radio frequency (RF) based technologies have been widely investigated for wireless access, including WiFi [9], WiMax [10] and radio-over-fiber (RoF) [11–13]. However, the capacity of widely used WiFi and WiMax is very limited and the RoF systems only have a license-free bandwidth of about 7 GHz in the 60 GHz frequency region. Furthermore, RF radiation inevitably produces severe electromagnetic interference (EMI) which is strictly prohibited in many areas such as hospitals and aircraft cabins.

As a promising alternative and complementary technology to RF based wireless communication, lightwave based optical wireless communication (OWC), including infrared communication and white light-emitting diode (LED) enabled visible light communication (VLC), has revealed great potential for providing high-speed and EMI-free wireless access in both outdoor [14,15] and indoor environments [16,17]. Since installation of fiber is not always achievable in remote, low-density areas or complex areas where installation of aerial or underground cables is limited due to either technical or economic limitations [15], outdoor OWC can provide high-speed wireless access to these underserved areas. Moreover, thanks to the rapid development of illumination LEDs, indoor OWC reveals great potential to provide high-speed indoor wireless connection using the existing lighting fixtures [17]. Therefore, it is of great significance to integrate OWC with PON systems to achieve high-speed hybrid wired and wireless optical access for end users. So far, only several integration schemes have been reported in literature. In [18], an integrated PON and OWC system was demonstrated based on a multiband single-carrier frequency domain equalization (SC-FDE) modulation technique. The signals for wired and wireless access are carried by different subbands and an electrical low-pass filter (LPF) is used to separate the wired signal and wireless signal in each optical network unit (ONU). Since OFDM is a better choice for multiuser PON systems [8], a service-integrated OFDM-PON system was proposed based on an on-off keying (OOK) overlaid OFDM modulation [19]. The

* Corresponding author.
E-mail addresses: chen0884@e.ntu.edu.sg (C. Chen), ewdzhong@ntu.edu.sg (W.-D. Zhong).

http://dx.doi.org/10.1016/j.optcom.2016.06.064
0030-4018/

low-speed OOK signal for wireless access is overlaid on the envelope of the high-speed OFDM signal for wired access. Nevertheless, the envelope of the OFDM signal fluctuates significantly due to the high peak-to-average power ratio (PAPR) which introduces inherent amplitude distortion to the overlaid OOK signal. In addition, since each OOK symbol is encoded to the envelope of one OFDM symbol, the OOK signal has the same symbol rate as the OFDM signal which might not be compatible with practical outdoor or indoor OWC links.

Recently, we have proposed a hybrid indoor access network (HIAN) which seamlessly integrates indoor OWC with WDM-PON based on a hierarchically modulated constant envelope OFDM (CE-OFDM) scheme and the preliminary results have been reported in [20]. In this paper, we investigate and analyze the bit-error rate (BER) performance of our recently proposed integrated variable-rate OWC and OFDM-PON system for hybrid wired and wireless optical access, based on an adaptive envelope modulation technique. Both the outdoor and indoor wireless communications are considered in the integrated system. The data for wired access is carried by a conventional OFDM signal and the data for wireless access is carried by an *M*-ary pulse amplitude modulation (*M*-PAM) signal which is modulated onto the envelope of the OFDM signal. In order to achieve a constant envelope and thus eliminate the inherent amplitude distortions of the conventional OFDM signal [19], a CE-OFDM signal is generated by performing discrete phase modulation after conventional OFDM encoding [21–23]. By adaptively modulating the wireless *M*-PAM signal onto the flat envelope of the wired CE-OFDM signal, signals for hybrid wired and wireless optical access can be seamlessly integrated. Furthermore, variable-rate OWC wireless access can be successfully achieved by using adaptive envelope modulation in the optical line terminal (OLT).

The rest of the paper is organized as follows. Section 2 describes the concept, system architecture and two key techniques, i.e. CE-OFDM and adaptive envelope modulation, of the integrated OWC and OFDM-PON system. In Section 3, analytical BER expressions of the CE-OFDM signal with *M*-PAM overlay and the overlaid *M*-PAM signal are derived and further verified by Monte Carlo simulations. The performance trade-off between the CE-OFDM signal with *M*-PAM overlay and the overlaid *M*-PAM signal is considered. The BER performances of wired access, indoor OWC wireless access and outdoor OWC wireless access are evaluated separately, and variable-rate OWC wireless access is also investigated. Finally, Section 4 concludes the paper.

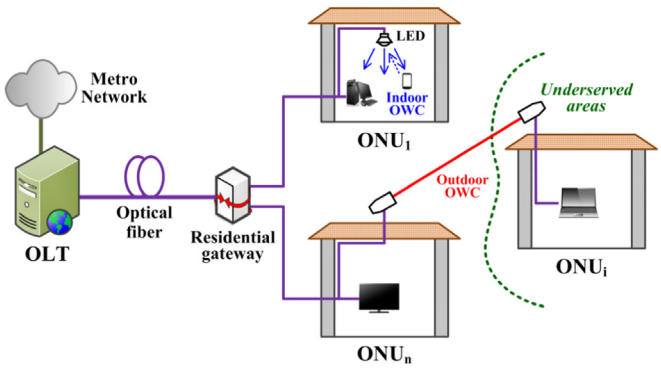

Fig. 1. Conceptual diagram of the integrated OWC and OFDM-PON system.

2. Integrated OWC and OFDM-PON system

2.1. Concept and system architecture

Fig. 1 illustrates the conceptual diagram of the integrated OWC and OFDM-PON system for hybrid wired and wireless optical access. The signal coming from the OLT passes through an optical fiber and a residential gateway is used to distribute the signal to the ONUs. In each ONU, wired services can be accessed by connecting optical fibers, and wireless services can be accessed through indoor OWC by using white illumination LEDs in the ceiling. Moreover, wireless access can also be achieved for the ONUs in the underserved areas through outdoor OWC.

The architecture of the integrated OWC and OFDM-PON system is shown in Fig. 2(a). In the OLT, the wired input data are encoded into a CE-OFDM signal. After adding a DC bias, a unipolar CE-OFDM signal is obtained. The wireless input data are modulated onto the envelope of the unipolar CE-OFDM signal through adaptive envelope modulation, where the wireless input data are first encoded into an *M*-PAM signal before envelope modulation. As a result, the wired input data and the wireless input data are simultaneously carried by the envelope-modulated CE-OFDM signal. The digital signal is further converted to an analog signal via digital-to-analog conversion (D/A) and the resultant signal is used to drive a laser diode (LD). After being transmitted over a single mode fiber (SMF), the optical signal is broadcasted to all the ONUs through an optical splitter (OS). In each ONU, another OS is used to divide the received optical signal into two branches. As shown in Fig. 2(a), one branch for wired access is received by a fast/high-bandwidth photodiode (PD) in which the envelope-modulated CE-OFDM signal is fully detected. After analog-to-digital conversion (A/D), the digital signal is fed into a CE-OFDM demodulator to generate the wired output data. The other branch for either indoor OWC wireless access or outdoor OWC wireless access is received by a slow/low-bandwidth PD in which envelope detection is performed and only the overlaid *M*-PAM signal is detected. For indoor OWC wireless access, a DC bias is first added to the *M*-PAM signal and the obtained unipolar *M*-PAM signal is used to drive an LED lamp. After indoor free-space transmission, the light is concentrated by a lens and then detected by a PD. The electrical *M*-PAM signal is A/D converted and demodulated to generate the wireless output data. For outdoor OWC wireless access, similarly, a DC bias is added to the *M*-PAM signal and the obtained unipolar *M*-PAM signal is used to drive an LD. The optical *M*-PAM signal is launched into the outdoor atmospheric turbulence channel through a transmit aperture (TA). After the outdoor free-space transmission, the light is captured by a receive aperture (RA) and then detected by a PD. The wireless output data are generated via A/D conversion and PAM demodulation. It should be noted that no optical or electrical filters are used in the ONUs and the signals for wired access and wireless access are separated by using two PDs with different bandwidths.

2.2. CE-OFDM

Instead of conventional OFDM which usually has a relatively large PAPR, the CE-OFDM scheme is adopted in the integrated OWC and OFDM-PON system thanks to its constant envelope characteristic. In the CE-OFDM modulator, the wired input data are first fed into a conventional OFDM modulator and thus a real-valued bipolar OFDM signal is generated. Then, the resultant OFDM signal is used to modulate the phase of a local oscillator (LO) in a phase modulator, resulting in a bipolar CE-OFDM signal which can be represented by [21]

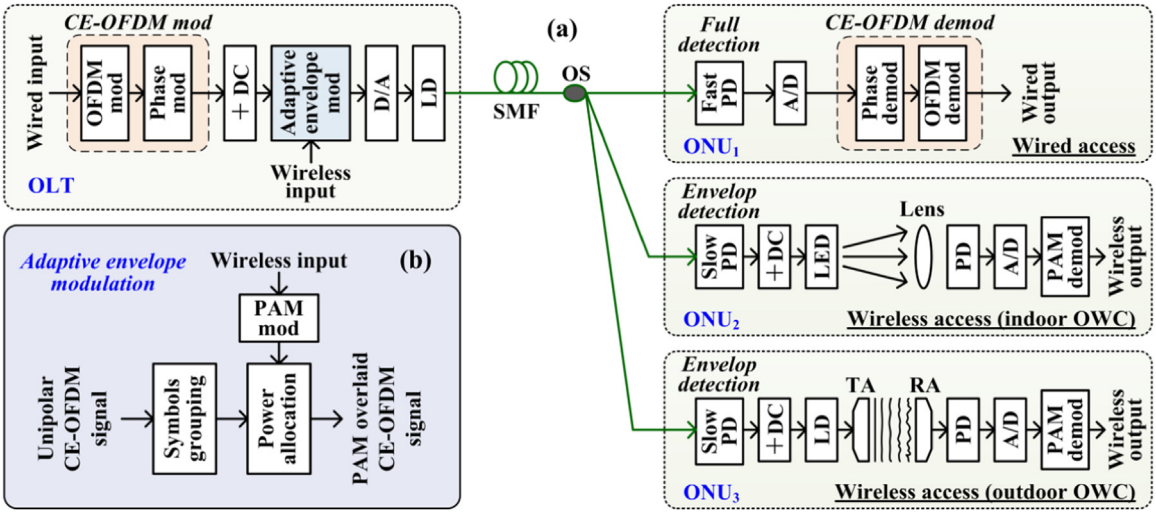

Fig. 2. (a) Architecture of the integrated OWC and OFDM-PON system and (b) inset: principle of adaptive envelope modulation.

$$S_{\mathrm{bi}}(t)=\Re\left\{ Ae^{j\varphi(t)}e^{j2\pi f_c t}\right\} = A\cos\left[2\pi f_c t+\varphi(t)\right], \tag{1}$$

where A is the signal amplitude, f_c is the carrier frequency of the LO and $\varphi(t)$ is the phase signal. During the ith symbol, $\varphi(t)$ is given by

$$\varphi(t) = \mu_{\mathrm{e}} C_{\mathrm{N}} m_i(t) + \theta_i, \tag{2}$$

where $\mu_{\mathrm{e}}=2\pi h$ is the electrical modulation index, C_{N} is a normalizing constant, $m_i(t)$ is the OFDM signal in the symbol and θ_i is a memory term which is set to make the modulation phase-continuous [21–23]. In the CE-OFDM demodulator, the received CE-OFDM signal is first phase-demodulated to recover the conventional OFDM signal which is then demodulated in a conventional OFDM modulator to obtain the wired output data.

2.3. Adaptive envelope modulation

The principle of adaptive envelope modulation is shown in the inset in Fig. 2, see Fig. 2(b). In order to perform adaptive envelope modulation, a non-negative or unipolar CE-OFDM signal is first generated by adding a DC bias to the bipolar CE-OFDM signal which is given by

$$S_{\mathrm{uni}}(t) = S_{\mathrm{bi}}(t) + DC = A\cos\left[2\pi f_c t+\varphi(t)\right] + DC. \tag{3}$$

In the adaptive envelope modulation, multiple consecutive unipolar CE-OFDM symbols are grouped together via symbols grouping and the power of each CE-OFDM symbol group is determined by the M-PAM encoded wireless input data via power allocation.

Fig. 3(a) illustrates the time trace of the M-PAM overlaid CE-OFDM signal. As we can see, n consecutive CE-OFDM symbols form one CE-OFDM symbol group and each CE-OFDM symbol group represents one M-PAM symbol, i.e., one M-PAM symbol occupies n complete CE-OFDM symbols. For the M-ary PAM modulation, the peak amplitude A_i of each CE-OFDM symbol group takes values from the discrete set $\{A_1, A_2,\cdots,A_M\}$ with $M \geq 2$, which can be represented by

$$A_i = A_1 + \frac{i-1}{M-1}(A_M - A_1), \tag{4}$$

where A_1 and A_M are the lowest and highest peak amplitudes of all the CE-OFDM symbol groups, respectively. Assuming that $DC = A$, as per (3) we have $A_M=2A$. Here, we define the peak amplitude ratio between the lowest peak A_1 and the highest peak A_M as

$$\alpha = \frac{A_1}{A_M}. \tag{5}$$

Since $0\leq A_1 \leq A_M$, we have $0 \leq \alpha \leq 1$. As per (4) and (5), A_i can be rewritten by

$$A_i = \frac{K_i}{M-1}A_M, \tag{6}$$

where $K_i=\alpha M - 1+(1-\alpha)i$. The time trace of the obtained M-PAM

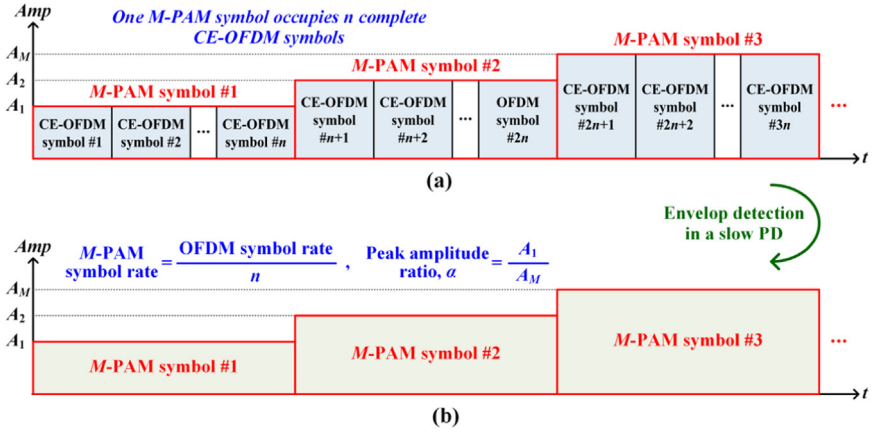

Fig. 3. Time traces of (a) M-PAM overlaid CE-OFDM signal after adaptive envelope modulation and (b) the obtained M-PAM signal after envelope detection in a slow PD.

signal after envelope detection in a slow/low-bandwidth PD is shown in Fig. 3(b). Since one M-PAM symbol occupies n consecutive CE-OFDM symbols, the relationship between the symbol rate of the M-PAM signal, $R^s_{M-\mathrm{PAM}}$, and the symbol rate of the CE-OFDM signal, $R^s_{\mathrm{CE-OFDM}}$, is given by

$$R^s_{M-\mathrm{PAM}} = \frac{R^s_{\mathrm{CE-OFDM}}}{n}. \tag{7}$$

For a fixed $R^s_{\mathrm{CE-OFDM}}$, $R^s_{M-\mathrm{PAM}}$ can be adjusted by varying the value of n.

3. Performance analysis

In this section, we analyze and evaluate the bit-error-rate (BER) performance of the integrated OWC and OFDM-PON system. Generalized BER expressions of both the CE-OFDM signal with M-PAM overlay and the overlaid unipolar M-PAM signal are first derived. Monte Carlo simulations are then performed to verify the validity of the theoretical derivations. In the integrated system, the received CE-OFDM signal is directly demodulated to obtain the wired output data, while the received M-PAM signal is further processed before indoor or outdoor OWC wireless transmission. Generally, there are two ways to process the received M-PAM signal: one is to amplify the signal [18] and the other is to decode and regenerate the signal [24]. Although the former is simpler than the later, much better performance can be achieved by the latter since the errors caused by optical fiber transmission can be corrected by using forward error correction (FEC) coding and hence error propagation from optical fiber transmission to OWC wireless transmission can be eliminated [24]. Due to its enhanced error performance, the latter is adopted in our following analysis. We first analyze the BER of the CE-OFDM signal with M-PAM overlay for wired access in Subsection 3.1. To optimize the overall performance of the integrated system, the BER of the overlaid M-PAM signal without OWC wireless transmission is also analyzed in this subsection. Performance trade-off between the CE-OFDM signal with M-PAM overlay and the overlaid M-PAM signal without OWC wireless transmission is then investigated. After that, the BER performances of indoor and outdoor OWC wireless access are presented in Subsections 3.2 and 3.3, respectively. Variable-rate indoor or outdoor OWC wireless access based on the adaptive envelope modulation technique is discussed in Subsection 3.4.

3.1. BER of wired access

3.1.1. BER of the CE-OFDM signal with M-PAM overlay

Making use of a high carrier-to-noise ratio (CNR) approximation, i.e. CNR $\geq$ 10 dB as discussed in [21], the BER of M_0-ary QAM based bipolar CE-OFDM signal over an additive white Gaussian noise (AWGN) channel can be approximated by [21]

$$BER^{\mathrm{bi}}_{\mathrm{CE-OFDM}} \approx \frac{2\left(\sqrt{M_0}-1\right)}{\sqrt{M_0}\log_2\sqrt{M_0}} Q\left(\mu_e\sqrt{\frac{6SNR_{\mathrm{bi}}}{M_0-1}}\right), \tag{8}$$

where $Q(\bullet)$ denotes the Q-function and SNR_{bi} denotes the electrical SNR per symbol of the bipolar CE-OFDM signal. Since real-valued and oversampled OFDM signals are generally transmitted in IM/DD based optical systems, the input to the IFFT is a conjugate symmetric, zero-padded data vector [21]. The power of the bipolar carrier is calculated by $\frac{1}{T}\int_0^T S^2_{\mathrm{bi}}(t)dt = \frac{A^2}{2}$ and the CNR of a bipolar CE-OFDM signal without M-PAM overlay is given by [21]

$$CNR_{\mathrm{bi}} = \frac{A^2/2}{B_nN_0}, \tag{9}$$

where B_n is the noise bandwidth and N_0 is the noise power spectrum density. Given an oversampling factor of J, the electrical SNR of the bipolar CE-OFDM signal can be calculated by [23, p. 67]

$$SNR_{\mathrm{bi}} = J\times CNR_{\mathrm{bi}} = \frac{JA^2}{2B_nN_0}. \tag{10}$$

After adding a DC bias A, a unipolar CE-OFDM signal $S_{\mathrm{uni}}(t)$ is obtained with A_M=2A and the power of the unipolar carrier is calculated by $\frac{1}{T}\int_0^T S^2_{\mathrm{uni}}(t)dt = \frac{3A^2}{2}$. Hence, the SNR of the unipolar CE-OFDM signal SNR_{uni} can be similarly calculated by

$$SNR_{\mathrm{uni}} = J\times CNR_{\mathrm{uni}} = J\times\frac{3A^2}{2B_nN_0} = \frac{3JA_M^2}{8B_nN_0} = 3SNR_{\mathrm{bi}}. \tag{11}$$

As per (11), the electrical SNR of the unipolar CE-OFDM signal is thrice as high as that of the bipolar CE-OFDM signal, which is proportional to the square of A_M for a given oversampling factor J and a fixed noise power B_nN_0. Throughout this paper, the electrical SNR of the unipolar CE-OFDM signal SNR_{uni} is adopted as a common metric to evaluate and compare the BER performance of the received CE-OFDM signal and the overlaid MPAM signal. Replacing SNR_{bi} in (8) with SNR_{uni}, the BER of the M_0-QAM based unipolar CE-OFDM signal is approximately given by

$$BER^{\mathrm{uni}}_{\mathrm{CE-OFDM}} \approx \frac{2\left(\sqrt{M_0}-1\right)}{\sqrt{M_0}\log_2\sqrt{M_0}} Q\left(\mu_e\sqrt{\frac{2SNR_{\mathrm{uni}}}{M_0-1}}\right). \tag{12}$$

After adaptive envelope modulation, the unipolar CE-OFDM signal is overlaid with a low-speed M-PAM signal and the peak amplitude of each CE-OFDM symbol group is given by (6). Hence, the electrical SNR of CE-OFDM symbols with the peak amplitude of A_i can be expressed by

$$SNR^i_{\mathrm{CE-OFDM}} = \frac{3JA_i^2}{8B_nN_0} = \left(\frac{K_i}{M-1}\right)^2\frac{3JA_M^2}{8B_nN_0}. \tag{13}$$

As per (11), we have

$$SNR^i_{\mathrm{CE-OFDM}} = \left(\frac{K_i}{M-1}\right)^2 SNR_{\mathrm{uni}}. \tag{14}$$

Substituting (14) into (12) yields the corresponding BER

$$BER^i_{\mathrm{CE-OFDM}} \approx \frac{2\left(\sqrt{M_0}-1\right)}{\sqrt{M_0}\log_2\sqrt{M_0}} Q\left(\frac{\mu_eK_i}{M-1}\sqrt{\frac{2SNR_{\mathrm{uni}}}{M_0-1}}\right). \tag{15}$$

Assuming that all the constellation points of M-PAM encoding are equiprobable, the overall BER of the M_0-QAM based CE-OFDM signal with M-PAM overlay can be expressed by

$$BER_{\mathrm{CE-OFDM}} = \frac{1}{M}\sum_{i=1}^{M} BER^i_{\mathrm{CE-OFDM}}. \tag{16}$$

3.1.2. BER of the overlaid M-PAM signal without OWC wireless transmission

Following the steps in [25, p. 163–164], we further derive the BER expression of the overlaid M-PAM signal without OWC wireless transmission. The amplitude of the unipolar M-PAM signal is obtained in (6) and thus the constellation of the overlaid unipolar M-PAM signal can be designed as

$$C_i = (i-1)l,\ i=1,\ 2,\ \cdots M, \tag{17}$$

where l is the distance between two nearest constellation points

$$l = \frac{A_M - A_1}{M-1} = \frac{1-\alpha}{M-1}A_M. \tag{18}$$

Then, the BER of the M-PAM signal over an AWGN channel is computed by [25, p. 163]

$$BER_{M-\mathrm{PAM}} = \frac{2(M-1)}{M\log_2 M} Q\left(\sqrt{\frac{l^2}{2N_0}}\right). \tag{19}$$

Since all M-PAM constellation points have an identical probability, the average symbol energy for the M-PAM signal is given by

$$E_S = \frac{1}{M}\sum_{i=1}^{M} C_i^2 = \frac{l^2}{M}\sum_{i=1}^{M}(i-1)^2. \tag{20}$$

Thus, replacing l in (19) with E_S, the BER can be written as

$$\begin{aligned} BER_{M-\mathrm{PAM}} &= \frac{2(M-1)}{M\log_2 M} Q\left(\sqrt{\frac{MSNR_{\mathrm{av}}}{2\sum_{i=1}^{M}(i-1)^2}}\right) \\ &= \frac{2(M-1)}{M\log_2 M} Q\left(\sqrt{\frac{3SNR_{\mathrm{av}}}{(M-1)(2M-1)}}\right), \end{aligned} \tag{21}$$

where $SNR_{\mathrm{av}} = E_S/N_0$ is the average electrical SNR of the overlaid M-PAM signal. Note that (21) is equivalent to the BER expression of the unipolar MPAM signal obtained in [26]. As per (13), the electrical SNR of the overlaid M-PAM signal for the constellation point C_i can be defined by

$$SNR_{M-\mathrm{PAM}}^{i} = \frac{JC_i^2}{B_n N_0} = \left(\frac{1-\alpha}{M-1}\right)^2 (i-1)^2 \frac{JA_M^2}{B_n N_0}. \tag{22}$$

As per (11), we get

$$SNR_{M-\mathrm{PAM}}^{i} = \frac{8}{3}\left(\frac{1-\alpha}{M-1}\right)^2 (i-1)^2 SNR_{\mathrm{uni}}. \tag{23}$$

Thus, the average electrical SNR of the overlaid unipolar M-PAM signal is obtained as

$$SNR_{M-\mathrm{PAM}}^{\mathrm{av}} = \frac{1}{M}\sum_{i=1}^{M} SNR_{M-\mathrm{PAM}}^{i} = \frac{4(1-\alpha)^2(2M-1)}{9(M-1)} SNR_{\mathrm{uni}}. \tag{24}$$

Substituting (24) into (21) yields the overall BER of the overlaid unipolar M-PAM signal

$$BER_{M-\mathrm{PAM}} = \frac{2(M-1)}{M\log_2 M} Q\left(\frac{1-\alpha}{M-1}\sqrt{\frac{4}{3}SNR_{\mathrm{uni}}}\right). \tag{25}$$

Monte Carlo simulations are performed to verify the validity of the above theoretical derivations over an AWGN channel. In the simulations, we assume that a 4PAM signal is overlaid on the envelope of a 64QAM based CE-OFDM signal. The fast Fourier transform (FFT) size is 256 and the oversampling factor is 2. The symbol rate of the CE-OFDM signal is assumed to be 10 GS/s and the electrical modulation index of the CE-OFDM signal is set to 0.8. Totally 4000 symbols are transmitted over the AWGN channel and collected for BER calculation.

Fig. 4(a) shows the BER performance of the 64QAM based CE-OFDM signal with 4PAM overlay for different peak amplitude ratios. The solid lines show the theoretical results as per (16), while the markers give the simulation results. It is observed that the simulation results agree well with the theoretical ones when the electrical SNR is relatively large. However, for a small electrical SNR which also indicates a smaller CNR, the theoretical expression becomes less accurate due to its precondition of high CNR. It is also found out that the best BER performance is attained when the peak amplitude ratio is 1 (i.e., no M-PAM overlay). With the decrease of the peak amplitude ratio, the BER performance gets worse and an error floor around BER$=10^{-1}$ exhibits when the peak amplitude ratio is 0. Hence, in order to achieve a good performance of the M-PAM overlaid CE-OFDM signal, a high peak amplitude ratio should be considered. The BER performance of the overlaid 4PAM signal is shown in Fig. 4(b). As per (25), the theoretical results (shown as solid lines) closely match the simulation results (shown as the markers). In contrast to the 4PAM overlaid CE-OFDM signal, the lowest BER is achieved for a given electrical SNR when the peak amplitude ratio is 0. The BER gets higher when the peak amplitude ratio is increased and the BER will reach 0.5 when the peak amplitude ratio is 1. Therefore, a relatively low peak amplitude ratio should be used to guarantee a good performance of the overlaid M-PAM signal.

3.1.3. BER trade-off

Based on the analysis above, we can conclude that there is a BER performance trade-off between the M-PAM overlaid CE-OFDM signal and the overlaid M-PAM signal without OWC wireless transmission. In order to optimize the overall performance of the integrated OWC and OFDM-PON system, the peak amplitude ratio should be optimized and a reasonable optimization condition is to achieve equal BER for both the M_0-QAM based CE-OFDM signal with M-PAM overlay and the overlaid M-PAM signal without OWC wireless transmission. As per (16) and (25), it can be seen that the

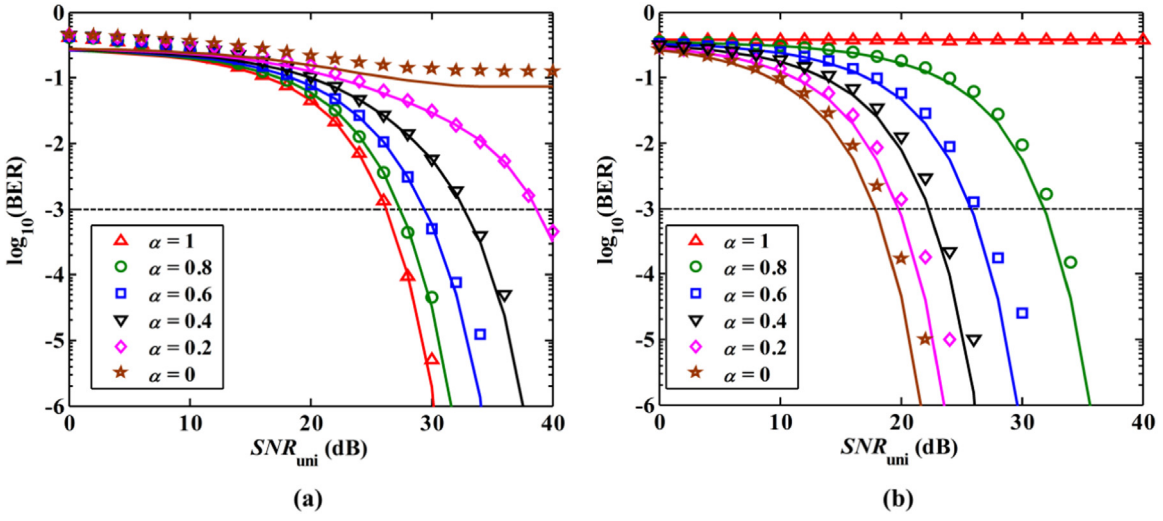

Fig. 4. BER vs. electrical SNR of the unipolar CE-OFDM signal for (a) 64QAM based CE-OFDM signal with 4PAM overlay and (b) the overlaid 4PAM signal without OWC wireless transmission. Markers and lines show the simulation and theoretical results, respectively.

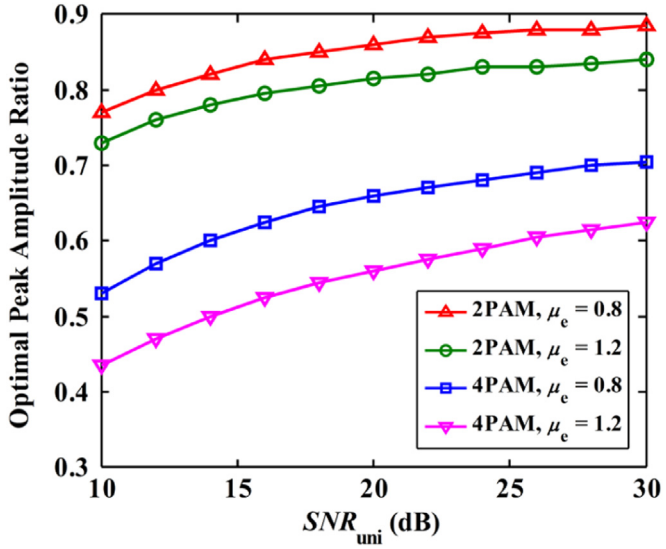

Fig. 5. Optimal peak amplitude ratio vs. electrical SNR of the unipolar CE-OFDM signal for 64QAM based CE-OFDM signal with *M*-PAM overlay.

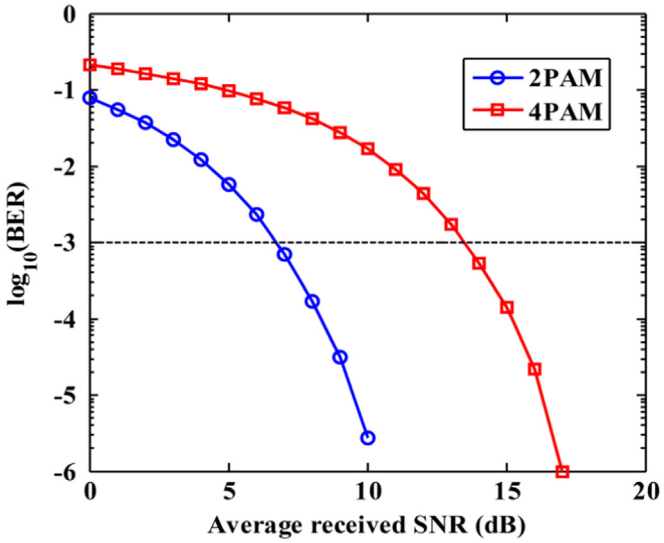

Fig. 6. BER vs. average received SNR for *M*-PAM based indoor OWC wireless access.

BER of the M_0-QAM based CE-OFDM signal with *M*-PAM overlay is a function of multiple variables including M_0, M, μ_e, SNR_{uni} and α, while the BER of the overlaid *M*-PAM signal is determined by the variables including M, SNR_{uni} and α.

We next examine the optimized peak amplitude ratio, α_{opt}, with the following parameters: M_0=64, M = 2or4, and μ_e=0.8 or 1.2. Fig. 5 shows the relationship between the optimal peak amplitude ratio and the electrical SNR. As can be seen in Fig. 5, the optimal peak amplitude ratio increases with the electrical SNR, and the optimal peak amplitude ratio for the case of 4PAM overlay is relatively lower than that for the case of 2PAM overlay. Furthermore, a smaller μ_e results in a higher optimal peak amplitude ratio. As per the results shown in Fig. 5, we can obtain the optimal peak amplitude ratio to reach the BER benchmark for the integrated OWC and OFDM-PON system. Assuming that a BER of 10^{-3} is set as the benchmark, the required SNR for the 64QAM based CE-OFDM signal with 4PAM overlay and μ_e=0.8 is about 27.4 dB, and thus the corresponding optimal peak amplitude ratio is found to be 0.69. Therefore, the performance of the integrated system can be optimized by selecting an optimal peak amplitude ratio. In addition, we can set the peak amplitude ratio to the optimal value when indoor or outdoor OWC based wireless link is activated (awake). However, when the wireless link is deactivated (sleep), the peak amplitude ratio can be set to 1 so as to reduce the required electrical SNR for wired access. By adaptively switching the value of peak amplitude ratio between its optimal value and 1, the energy efficiency of the integrated system can be substantially improved.

3.2. BER of indoor OWC wireless access

Since the errors caused by optical fiber transmission are corrected before indoor OWC wireless transmission, an error-free *M*-PAM signal is superimposed onto a DC bias, as shown in ONU_2 in Fig. 1, and the combined signal is used to drive the white LED. After propagating through an indoor optical wireless channel, the light is concentrated by an optical lens which is further detected by a PD. The resultant electrical *M*-PAM signal is demodulated to obtain the wireless output data.

The line-of-sight (LOS) irradiance of an LED can be modeled by a generalized Lambertian radiation pattern [27] and the LOS channel DC gain is given by

$$h=\begin{cases}\dfrac{(l+1)A}{2\pi d^2}\cos^l(\varphi)T_s(\theta)g(\theta)\cos(\theta), 0\le\theta\le\Theta_{1/2}\\ 0, \theta>\Theta_{1/2}\end{cases}, \tag{26}$$

where $l=-\ln 2/\ln\left(\cos\Psi_{\frac{1}{2}}\right)$ is the order of Lambertian emission and $\Psi_{1/2}$ is the transmitter semi-angle at half power. A is the active area of the detector, d is the distance, φ is the angle of irradiance, θ is the angle of incidence, and $T_s(\theta)$ is the gain of an optical filter. $g(\theta)$ and $\Theta_{1/2}$ are the gain and the field of view (FOV) of the optical lens, respectively.

We evaluate the BER performance of *M*-PAM based indoor OWC wireless access via Monte Carlo simulations with M = 2 and 4. The distance is set to be 3 m. The LED and the PD are located at the center of the ceiling and the floor, respectively. The other simulation parameters can be found in Table I of [27]. Fig. 6 shows the BER versus received SNR for *M*-PAM based indoor OWC wireless access. As can be seen, 2PAM requires a received SNR of about 6.7 dB to reach the BER benchmark of 10^{-3}, while a received SNR of about 13.5 dB is required for 4PAM.

3.3. BER of outdoor OWC wireless access

The performance of outdoor OWC wireless access, as shown in ONU_3 in Fig. 1, is highly affected by the atmospheric turbulence which could cause fluctuation of signal amplitude and hence distort the transmitted signal [28–30]. Similarly, an error-free *M*-PAM signal is transmitted through the turbulence channel. Outdoor OWC turbulence channel can be modeled by the Gamma–Gamma distribution which is expressed by [28]

$$f(I)=\frac{2(\alpha\beta)^{(\alpha+\beta)/2}}{\Gamma(\alpha)\Gamma(\beta)}I^{(\alpha+\beta)/2-1}K_{\alpha-\beta}\left(2\sqrt{\alpha\beta I}\right),\ I>0, \tag{27}$$

where α and β are the parameters of Gamma–Gamma distribution related to the large-scale and small-scale scintillation, respectively, $\Gamma(\bullet)$ is the Gamma function, $K_m(\bullet)$ is the second kind modified Bessel function of order m. Assuming that the optical radiation is a plane wave, α and β are respectively given by [30]

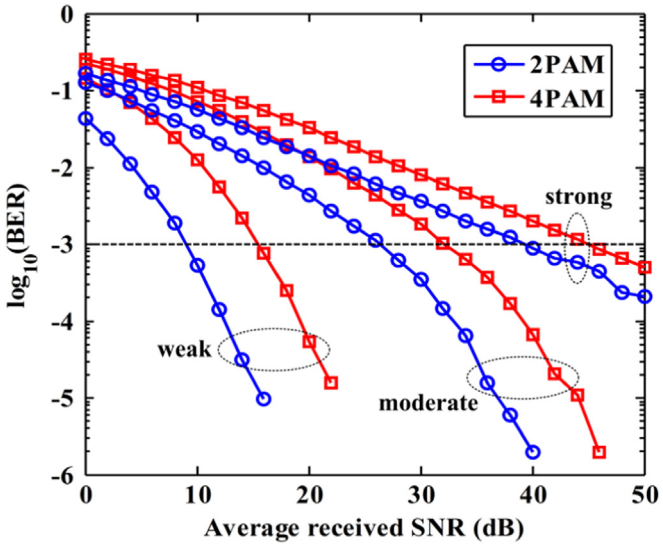

Fig. 7. BER vs. average received SNR for M-PAM based outdoor OWC wireless access under various turbulence conditions.

$$\alpha = \left\{ \exp\left[\frac{0.49\sigma_R^2}{(1+1.11\sigma_R^{12/5})^{7/6}} \right] - 1 \right\}^{-1}, \quad \beta = \left\{ \exp\left[\frac{0.51\sigma_R^2}{(1+0.69\sigma_R^{12/5})^{5/6}} \right] - 1 \right\}^{-1}, \tag{28}$$

where σ_R^2 is the Rytov variance, which is a general measure of atmospheric turbulence strength.

Fig. 7 shows the BER versus received SNR for M-PAM based outdoor OWC wireless access under various turbulence conditions. where the values of Rytov variance corresponding to the weak, moderate and strong turbulence conditions are 0.2, 1.2 and 4, respectively. As can be seen from Fig. 7, under the weak turbulence condition, the average received SNRs required by 2PAM and 4PAM to reach the BER benchmark of 10^{-3} are 9.1 dB and 15.5 dB, respectively. However, much higher SNRs are required for both 2PAM and 4PAM when the turbulence gets stronger.

3.4. Variable-rate OWC wireless access

In practical indoor or outdoor environments, the data rate of OWC wireless access might not be constant all the time. For example, the data rate of indoor OWC wireless access is affected by many factors such as user mobility and dimming control [16], while the data rate of outdoor OWC wireless access is mainly affected by the atmospheric turbulence, particularly in the presence of aerosols such as fog, smoke and dust [28,29]. Since the achievable data rate of OWC wireless access is variable in real implementation of OWC systems, the proposed adaptive envelope modulation technique which can support variable-rate OWC wireless access is highly desirable to fully exploit the capacity of indoor or outdoor OWC systems.

As shown in Fig. 2(b), the symbol rate of the overlaid M-PAM signal after adaptive envelope modulation is determined by (7) and the achievable bit rate of the overlaid M-PAM signal, $R_{M-\mathrm{PAM}}^{\mathrm{b}}$, is expressed by

$$R_{M-\mathrm{PAM}}^{\mathrm{b}} = R_{M-\mathrm{PAM}}^{\mathrm{s}} \log_2 M = \frac{R_{\mathrm{CE-OFDM}}^{\mathrm{s}} \log_2 M}{n}. \tag{29}$$

It can be seen that the achievable bit rate of the overlaid M-PAM signal is linearly proportional to $R_{\mathrm{CE-OFDM}}^{\mathrm{s}}$ and $\log_2 M$, which is also inversely proportional to the value of n. In practical scenarios,

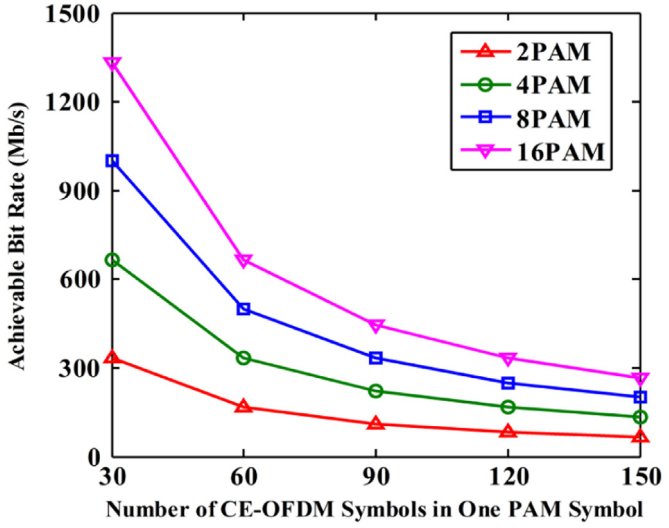

Fig. 8. Achievable bit rate of indoor or outdoor OWC wireless access vs. the number of CE-OFDM symbols in one PAM symbol.

$R_{\mathrm{CE-OFDM}}^{\mathrm{s}}$ can be assumed as a fixed value, thus M and n are the two parameters that can be adaptively adjusted to achieve variable-rate indoor or outdoor OWC wireless access. According to (29), the achievable bit rate in the unit of Mb/s is then given by $10^4 \log_2 M/n$.

Fig. 8 depicts the relationship between the achievable bit rate and the value of n for different PAM orders. Taking 8PAM for example, the achievable bit rate varies from 200 to 1000 Mb/s when the value of n is changed from 150 to 30. Therefore, by changing M or n, we can achieve variable bit rate indoor or outdoor OWC wireless access.

4. Conclusions

We have investigated an indoor integrated variable-rate OWC and OFDM-PON system where signals for both wired and wireless access are converged in the OLT and simultaneously delivered to each ONU over an optical fiber, by using the adaptive envelope modulation technique. Both the outdoor and indoor wireless communications are considered in the integrated system. Electrical or optical filtering is not required in the ONUs and two PDs with different bandwidths are employed to separate the different signals. Generalized BER expressions of the CE-OFDM signal with M-PAM overlay and the overlaid M-PAM signal have been derived and verified by Monte Carlo simulations. The BER performances of wired access, indoor OWC wireless access and outdoor OWC wireless access have been investigated separately, and variable-rate indoor or outdoor OWC wireless access has also been achieved by using the adaptive envelope modulation technique.

Acknowledgments

This work was supported by MOE/NTU AcRF Tier 1 Grant RG 85/13.

References

[1] S. Sarkar, S. Dixit, B. Mukherjee, Hybrid wireless-optical broadband-access network (WOBAN): a review of relevant challenges, J. Light. Technol. 25 (11) (2007) 3329–3340.
[2] L. Kazovsky, S.-W. Wong, T. Ayhan, K. Albeyoglu, M. Ribeiro, A. Shastri, Hybrid optical–wireless access networks, Proc. IEEE 100 (5) (2012) 1197–1225.
[3] F. Effenberger, H. Ichibangase, H. Yamashita, Advances in broadband passive

optical networking technologies, IEEE Commun. Mag. 39 (12) (2001) 118–124.
[4] Y.-L. Hsueh, M. Rogge, S. Yamamoto, L. Kazovsky, A highly flexible and efficient passive optical network employing dynamic wavelength allocation, J. Light. Technol. 23 (1) (2005) 277–286.
[5] C. Chen, C. Zhang, W. Zhang, W. Jin, K. Qiu, Scalable and reconfigurable generation of flat optical comb for WDM-based next-generation broadband optical access networks, Opt. Commun. 321 (2014) 16–22.
[6] C. Chow, C. Yeh, C. Wang, C. Wu, S. Chi, C. Lin, Studies of OFDM signal for broadband optical access networks, IEEE J. Sel. Areas Commun. 28 (6) (2010) 800–807.
[7] L. Zhang, X. Xin, B. Liu, Y. Wang, Secure OFDM-PON based on chaos scrambling, IEEE Photon. Technol. Lett. 23 (14) (2011) 998–1000.
[8] C. Chen, C. Zhang, D. Liu, K. Qiu, S. Liu, Tunable optical frequency comb enabled scalable and cost-effective multiuser orthogonal frequency-division multiple access passive optical network with source-free optical network units, Opt. Lett. 37 (19) (2012) 3954–3956.
[9] N. Ghazisaidi, M. Maier, C.M. Assi, Fiber-wireless (FiWi) access networks: a survey, IEEE Commun. Mag. 47 (2) (2009) 160–167.
[10] K. Yang, S. Ou, K. Guild, H.-H. Chen, Convergence of Ethernet PON and IEEE 802.16 broadband access networks and its QoS-aware dynamic bandwidth allocation scheme, IEEE J. Sel. Areas Commun. 27 (2) (2009) 101–116.
[11] G.-K. Chang, A. Chowdhury, Z. Jia, H.-C. Chien, M.-F. Huang, J. Yu, G. Ellinas, Key technologies of WDM-PON for future converged optical broadband access networks [Invited], J. Opt. Commun. Netw. 1 (4) (2009) C35–C50.
[12] C. Chen, C. Zhang, W. Zhang, W. Jin, K. Qiu, Hybrid WDM-OFDMA-PON utilising tunable generation of flat optical comb, Electron. Lett. 49 (4) (2013) 276–277.
[13] Y. Xiang, C. Chen, C. Zhang, K. Qiu, Wired/wireless access integrated RoF-PON with scalable generation of multi-frequency MMWs enabled by polarization multiplexed FWM in SOA, Opt. Exp. 21 (1) (2013) 1218–1225.
[14] C. Chen, W.-D. Zhong, D.H. Wu, MDPSK-Based nonequalization OFDM for coherent free-space optical communication, IEEE Photon. Technol. Lett. 26 (16) (2014) 1617–1620.
[15] V. Mai, A.T. Pham, Adaptive rate-based MAC protocols design and analysis for integrated FSO/PON networks, Proc. IEEE ICC (2015) 5007–5012.
[16] H. Elgala, R. Mesleh, H. Haas, Indoor optical wireless communication: potential and state-of-the-art, IEEE Commun. Mag. 49 (9) (2011) 56–62.
[17] H.L. Minh, D.C. O'Brien, G. Faulkner, L. Zeng, K. Lee, D. Jung, Y. Oh, E.T. Won, 100-Mbit/s NRZ visible light communications using a postequalized white LED, IEEE Photon. Technol. Lett. 21 (15) (2009) 1063–1065.
[18] Y. Wang, J. Yu, N. Chi, Symmetric full-duplex integrated passive optical network and optical wireless communication transmission system, J. Opt. Commun. Netw. 7 (7) (2015) 628–633.
[19] J.Y. Sung, C.W. Chow, C.H. Yeh, Y.C. Wang, Service integrated access network using highly spectral-efficient MASK-MQAM-OFDM coding, Opt. Exp. 21 (5) (2013) 6555–6560.
[20] W.-D. Zhong, C. Chen, D. Wu, Seamless integration of indoor VLC with WDM-PON based on hierarchically modulated constant envelope OFDM, in: Proc. ICTON, Mo.C2.2, 2015.
[21] S.C. Thompson, A.U. Ahmed, J.G. Proakis, J.R. Zeidler, M. Geile, Constant envelope OFDM, IEEE Trans. Commun. 56 (8) (2008) 1300–1312.
[22] R.B. Nunes, H.R. de O. Rocha, D.A.A. Mello, F.D. Simoes, M.E.V. Segatto, J.A. L. Silva, Transmission of CE-OFDM signals over MMF links using directly modulated 850-nm VCSELs, IEEE Photon. Technol. Lett. 27 (3) (2015) 315–318.
[23] S.C. Thompson, Constant envelope OFDM phase modulation (Ph.D. dissertation), University of California, San Diego, 2005.
[24] C.W. Chow, C.H. Yeh, Y. Liu, C.W. Hsu, J.Y. Sung, Network architecture of bidirectional visible light communication and passive optical network, IEEE Photon. J. 8 (3) (2016) 7904506.
[25] A. Goldsmith, Wireless Communications, Cambridge University Press, Cambridge, U.K., 2005.
[26] I.B. Djordjevic, G.T. Djordjevic, On the communication over strong atmospheric turbulence channels by adaptive modulation and coding, Opt. Exp. 17 (20) (2009) 18250–18262.
[27] C. Chen, W.-D. Zhong, D. Wu, Communication coverage improvement of indoor SDM-VLC system using NHS-OFDM with a modified imaging receiver, presented in ICC 2016.
[28] J. Libich, S. Zvanovec, Influences of turbulences in near vicinity of buildings on free-space optical links, IET Microw. Antennas Propag. 5 (9) (2011) 1039–1044.
[29] M. Ijaz, Z. Ghassemlooy, J. Perez, V. Brazda, O. Fiser, Enhancing the atmospheric visibility and fog attenuation using a controlled FSO channel, IEEE Photon. Technol. Lett. 25 (13) (2013) 1262–1265.
[30] M.A. Khalighi, M. Uysal, Survey on free space optical communication: a communication theory perspective, IEEE Commun. Surv. Tutor. 16 (4) (2014) 2231–2258.